Journal of Alloys and Compounds 892 (2021) 162045

Contents lists available at ScienceDirect

Journal of Alloys and Compounds

journal homepage: www.elsevier.com/locate/jalcom

Synthesis and thermoelectric properties of high-entropy half-Heusler $MFe_{1-x}Co_xSb$ (M = equimolar Ti, Zr, Hf, V, Nb, Ta)

Kan Chen[a,*], Ruizhi Zhang[a], Jan-Willem G. Bos[b], Michael J. Reece[a,*]

[a] School of Engineering and Materials Science, Queen Mary University of London, Mile End Road, London E1 4NS, UK
[b] Institute of Chemical Sciences and Centre for Advanced Energy Storage and Recovery, School of Engineering and Physical Sciences, Heriot-Watt University, Edinburgh EH14 4AS, UK

ARTICLE INFO

Article history:
Received 7 April 2021
Received in revised form 24 August 2021
Accepted 17 September 2021
Available online 24 September 2021

Keywords:
Intermetallics
Mechanical alloying
Sintering
Entropy
Thermoelectric
Heat conduction

ABSTRACT

The application of the high-entropy concept has generated many interesting results for both alloys and ceramics. However, there are very few reports on high entropy thermoelectric materials. In this work, a single phase high-entropy half-Heusler compound $MFe_{1-x}Co_xSb$ with 6 equimolar elements (Ti, Zr, Hf, V, Nb and Ta) on the M site was successfully synthesized by a simple method of mechanical alloying, and the single phase was maintained after densification by spark plasma sintering. The multi-elements are homogenously distributed in the samples. The samples are stable and there is no phase separation after annealing at 1073 K in argon for 72 h, which could be attributed to their high configurational entropy. Due to the phonon scattering introduced by multi-elements, the lattice thermal conductivity is largely suppressed with a lowest value of ~ 1.8–1.5 $Wm^{-1}K^{-1}$ (300–923 K) for MCoSb. By adjusting the Fe/Co ratio, the samples can show both n-type and p-type semiconductor behavior. Maximum zT values of 0.3 and 0.25 are achieved for n-type MCoSb and p-type $MFe_{0.6}Co_{0.4}Sb$, respectively. The results suggest that the high-entropy concept is a promising strategy to extend the composition range and tune the thermoelectric properties for half-Heusler materials, which could potentially be applied in other thermoelectric materials.

1. Introduction

Thermoelectric materials can realize direct conversion between heat and electricity, which is of great interest for both power generation and electrical cooling. The thermoelectric performance of a material can be quantified by its dimensionless figure-of-merit, which is defined as $zT = \alpha^2\sigma\kappa^{-1}T$, where α is the Seebeck coefficient, σ is the electrical conductivity, κ is the thermal conductivity and T is the absolute temperature [1,2]. κ comprises two parts, $\kappa = \kappa_e + \kappa_L$, where κ_e is the electronic thermal conductivity and κ_L is the lattice thermal conductivity. A good thermoelectric material should simultaneously possess a high power factor ($\alpha^2\sigma$) and low κ, but it is difficult to optimize the properties individually due to their strong interconnections [3].

Half-Heusler (HH) compounds have great potential for power generation in the mid temperature regime (700 – 1000 K), as they generally have high power factors, robust mechanical properties, good thermal stability, low-toxicity and relatively inexpensive constituent elements. Maximum zT values of ~1.6 were reported for half-Heusler compounds and, a high efficiency of ~11.4% was obtained at 973 K with a temperature gradient of 656 K [4–8]. HH compounds are intermetallics with a simple cubic structure. They have a general composition formula of XYZ, where X and Z occupy a NaCl lattice and Y occupies half of the tetragonal sites. For better interpretation of their semiconducting properties, HH compounds can be also described as partially ionic $X^{n+}(YZ)^{n-}$ based on the Zintl–Klemm concept. In this case, the most electropositive element X acts as a cation and donates all of its valence electrons, while (YZ) form a covalent tetrahedrally bonded sublattice and act as an anion, resulting in a similar electronic structure to that of ZnS [9]. Based on the Zintl concept, a 18 valence electron count (VEC) per unit cell can be used to guide the identification of stable HH compounds as potential thermoelectric materials. MNiSn (n-type) and MCoSb (p-type) (M = Ti, Zr, Hf) are the most common HH compounds with a 18 VEC. They have been studied intensively and high zT values over 1 have been reported for both n- and p-type HH compounds [10–13]. Some other 18 VEC HH compounds have also been reported, such as NbFeSb [14,15], NbCoSn [16], VFeSb [17], ZrCoBi [18,19] and TaFeSb [8]. Besides, there are many predicted 18 VEC HH compounds that have not been reported experimentally [20].

* Corresponding authors.
E-mail addresses: kan.chen@qmul.ac.uk (K. Chen), m.j.reece@qmul.ac.uk (M.J. Reece).

https://doi.org/10.1016/j.jallcom.2021.162045
0925-8388/

The vast variety of HH compounds with simple crystal structure motivates the idea of applying the high-entropy concept to the HH system. The high-entropy concept was first demonstrated in metal alloys that are composed of five or more elements in equimolar ratio, such as CuCoNiCrAlFe, FeCrMnNiCo and TiZrHfNbTa [21–23], which show interesting mechanical properties. The high-entropy concept has now been applied to other high-entropy compounds (HECs), including oxides [24,25], nitrides [26], carbides [27,28], borides [29], and chalcogenides [30,31]. In these compounds, the equimolar elements are on the cation sublattice, and their large configurational entropy contributes to their formation as a single-phase [32]. Compared to the conventional solid-solutions with low amounts of additions, the high-entropy effect with equimolar components can overcome limited solubilities and structural mismatches. It was first demonstrated by synthesizing an equimolar mixture of MgO, CoO, NiO, CuO and ZnO, in which the limited solubilities of MgO–ZnO and CuO–NiO and the structural mismatches of tenorite CuO and wurtzite ZnO were overcome by the entropy effect, and a single-phase (MgCoNiCuZn)O with a rock-salt structure was formed [25]. The study of HECs has generated interesting results in different fields, such as dielectrics [33], Li-ion battery [34,35], ultra-high temperature ceramics [27], and thermoelectrics [31]. In terms of HH thermoelectrics, the high-entropy concept could be an effective way to reduce their lattice thermal conductivity. HHs have relatively high thermal conductivities (10–20 $Wm^{-1}K^{-1}$ at 300 K for typical unalloyed compositions) which limits their zT values. An overview of the κ_L of some of the end-member HH alloys used here is given in Fig. 5(c). The multi-elements in the X sublattice will introduce point defects, mass contrast, structural complexity and possibly local phase separation, which could all contribute to the suppression of κ_L. Recently, there are two reports related to high-entropy HH compounds. Yan et.al. reported $Nb_{1-x}M_xFeSb$ (M = Ti, V, Hf, Mo and Zr with an equimolar ratio) HH compounds [36]. The reported samples contained an impurity of $NbSb_2$ and the multiple elements were not homogeneously distributed. However, there is an obvious reduction in the lattice thermal conductivity (κ_L is reduced by ~56% in x = 0.4 sample) and also an increase in hardness. Karati et.al. reported a $Ti_2NiCoSbSn$ HH compound that was claimed to be a high-entropy alloy, but it only contains at most 2 elements per atomic site [37]. The samples contained impurities of TiC and Sn and showed poor thermoelectric performance, but they found that the use of multi-elements improved the synthesisability and extended the solid solubility limits. Due to the limited research, it is still not clear what is the effect of the high-entropy approach on the synthesisability and properties of HH compounds.

In this work we investigated the synthesisability and thermoelectric properties of high-entropy HH compounds with six equimolar elements on the cation sublattice, of which the designed composition is $MFe_{0.5}Co_{0.5}Sb$ (M = equimolar Ti, Zr, Hf, V, Nb, Ta) with a 18 VEC. As Sb-based HH compounds show very promising thermoelectric performance, the composition is based on six simple HH compounds of TiCoSb, ZrCoSb, HfCoSb, VFeSb, NbFeSb and TaFeSb. All of these compounds have the same crystal structure and a 18 VEC. A schematic crystal structure of $MFe_{0.5}Co_{0.5}Sb$ is shown in Fig. 1, showing the mix of elements on the individual sites. The ideal configurational entropy of a compound with different cation sites and anion sites can be calculated using the following equation:

$$\Delta S_{mix} = -R\left[\left(\sum_{h=1}^{M} x_h \ln x_h\right)_{\text{X-site}} + \left(\sum_{i=1}^{N} x_i \ln x_i\right)_{\text{Y-site}} + \left(\sum_{j=1}^{L} x_j \ln x_j\right)_{\text{Z-site}}\right]$$

where R is the gas constant, M, N and L are the number of constituent elements on X, Y and Z sites, and x_h, x_i and x_j are the mole fraction of elements on X, Y and Z sites [38]. For $MCo_{0.5}Fe_{0.5}Sb$, the ideal configurational entropy is 2.485 R, which can be classified as high-entropy. The atomic radius of the smallest atom (V) and the largest atom (Zr) differ by more than 15%, which is not favorable to form a solid solution as suggested by the Hume-Rothery rule [39], but a single phase $MFe_{0.5}Co_{0.5}Sb$ was formed by using the simple processing method of ball-milling (BM) the constituent elements, and there was no phase separation or impurity in the sample after sintering by using spark plasma sintering (SPS). $MFe_{0.5}Co_{0.5}Sb$ has n-type semiconducting behavior and a very low lattice thermal conductivity of ~ 2.2 $Wm^{-1}K^{-1}$ at 300 K and ~1.8 $Wm^{-1}K^{-1}$ at 923 K. The thermoelectric performance of $MFe_{0.5}Co_{0.5}Sb$ was improved by tuning the Fe/Co ratio. Moreover, the $MFe_{1-x}Co_xSb$ system showed great tunability as a pure HH phase was maintained with VEC from 17.9 to 18.5, and the system can behave as both n- and p-type depending on the VEC.

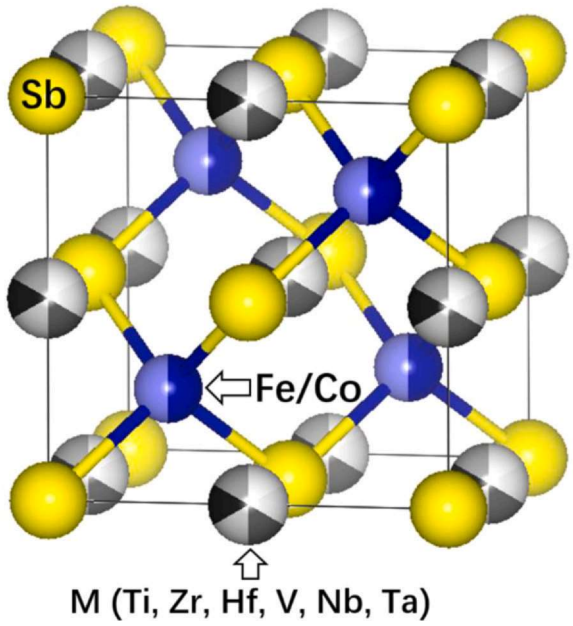

Fig. 1. Schematic crystal structure of $MCo_{1-x}Fe_xSb$. M is equimolar Ti, Zr, Hf, V, Nb, Ta which form a high-entropy sublattice.

2. Experimental details

Polycrystalline $MFe_xCo_{1-x}Sb$ (M = equimolar Ti, Zr, Hf, V, Nb, Ta) samples were prepared by BM + SPS. Starting powders of Ti (- 325 mesh, 99.99%, Alfa Aesar), Zr (- 325 mesh, 98.8%, Alfa Aesar), Hf (- 325 mesh, 99.6%, Alfa Aesar), V (- 325 mesh, 99.5%, Alfa Aesar), Nb (-325 mesh, 99.8%, Alfa Aesar), Ta (-325 mesh, 99.97%, Alfa Aesar), Fe (< 10 µm, 99.9+ %, Alfa Aesar), Co (-100 + 325 mesh, 99.8%, Alfa Aesar) powder and Sb (- 100 mesh, 99.5%, Alfa Aesar) were weighed according to the required stoichiometric ratios and ball-milled in a planetary ball mill machine (PULVERISETTE 5/4, Fritsch, Germany) in argon at a rotation speed of 300 rpm for 400 min. The ball-milled powders were sintered at 1173 K for 5 min at a pressure of 60 MPa using a SPS furnace (FCT HPD 25, FCT System GmbH, Germany). The phases of the samples were examined using X-ray powder diffraction (XRD, PANalytical X'Pert Pro, CuKα). The microstructures and compositions were investigated using scanning electron microscopy (SEM, FEI, Inspect F, 10 kV). Secondary electrons images were taken of freshly fractured surfaces, while backscattered electron imaging and energy-dispersive X-ray spectroscopy (EDX) mapping were performed on polished surfaces. The electrical conductivity and Seebeck coefficient were measured using a commercial instrument (LSR-3/110, Linseis) in a He atmosphere up to 923 K. The uncertainty of the electrical conductivity and Seebeck coefficient values is less than 5%. The thermal diffusivity was measured using the flash diffusivity method (LFA 457, Netzsch) up to 923 K. The specific heat

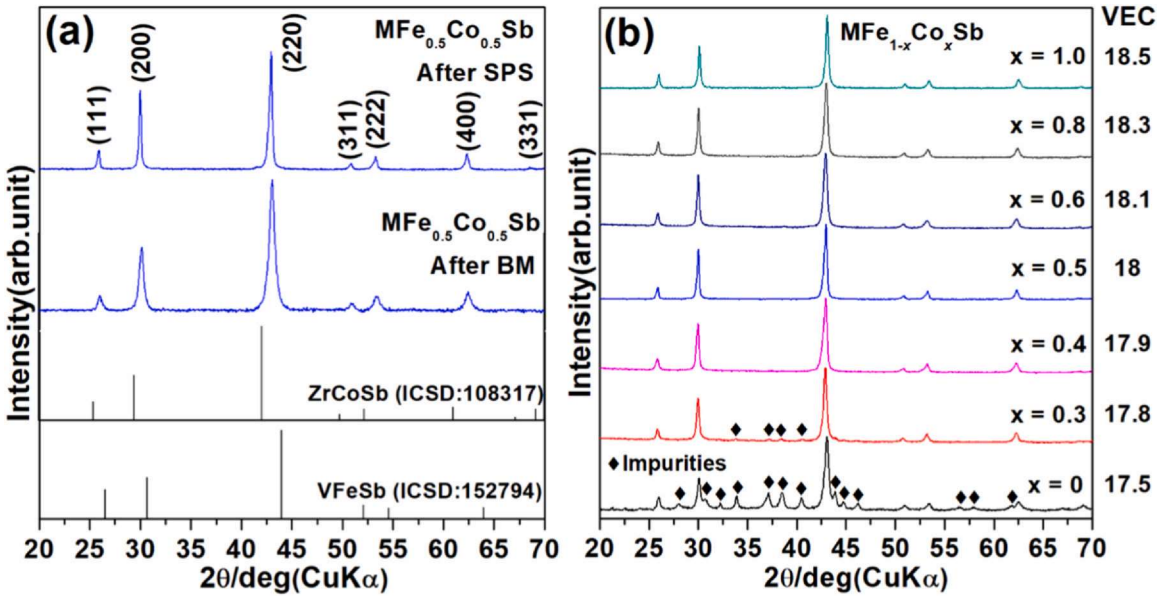

Fig. 2. (a) XRD patterns of $MFe_{0.5}Co_{0.5}Sb$ after BM and after SPS and (b) XRD patterns of $MFe_{1-x}Co_xSb$ after SPS (M = equimolar Ti, Zr, Hf, V, Nb, Ta).

capacity (C_p) was estimated using the Dulong-Petit law. The uncertainty of thermal diffusivity measurements was less than 5%. The density was measured using the Archimedes method with an uncertainty of less than 1%, and all the samples have a relative density greater than 99%. The thermal conductivity was calculated using the thermal diffusivity, specific heat capacity and density.

3. Results and discussion

Fig. 2(a) shows the XRD patterns of the high-entropy HH $MFe_{0.5}Co_{0.5}Sb$ (M = equimolar Ti, Zr, Hf, V, Nb, Ta) samples after BM and after SPS. The $MFe_{0.5}Co_{0.5}Sb$ compound exhibited a cubic structure with space group of $\bar{F}43m$. The samples after BM and after SPS were both single phase and no impurity was observed within the detection limit of XRD. Reference data for VFeSb (ICSD:152794) and ZrCoSb (ICSD:108317) are included for comparison. In all six related ternary HH compounds, VFeSb has the smallest lattice parameter a = 5.823 Å while ZrCoSb has the largest lattice parameter a = 6.068 Å. All of the peaks of $MFe_{0.5}Co_{0.5}Sb$ are in between those of VFeSb and ZrCoSb and its lattice parameter is a = 5.956 Å, which indicates it formed a solid solution with a HH phase structure. The relative density of $MFe_{0.5}Co_{0.5}Sb$ after SPS was 99.4% based on a theoretical density of 8.95 g/cc calculated using the XRD data. It is worth noting that single phase $MFe_{0.5}Co_{0.5}Sb$ was achieved by a simple and scalable processing method of ball-milling at 300 rpm for a short period time of 400 mins, in contrast to the traditional synthesis method used for HH compounds, which involves melt processing and long-time (often days) annealing. Also, the sample is reproducible and the XRD results of two batches of $MFe_{0.5}Co_{0.5}Sb$ are shown in Fig. S1 (Support information), which reveals nearly identical diffraction patterns. The six equimolar elements in the X cation sublattice, which have large configurational entropy, could contribute to the formation of a single-phase and the improved synthesisability of $MFe_{0.5}Co_{0.5}Sb$ compared to simple HH compounds. Fig. 2(b) shows the XRD patterns of a series of samples of $MFe_{1-x}Co_xSb$ (x = 0 ~1) after SPS. It can be seen that the structure can accommodate more Co than Fe on the Y site. A single phase was achieved with only Co on the Y site (MCoSb), while a small amount of impurity starts to form in $MFe_{0.7}Co_{0.3}Sb$ that is more obvious in MFeSb. A solid solution of $(Ti,Zr,Hf)CoSb_{0.9}Sn_{0.1}$ with 3 elements on the X site was reported by Rausch et. al, and there was an obvious impurity and also phase separation [40]. These observations suggest that high-entropy may contribute to the formation of a single phase MCoSb with 6 elements on the X site. As Co has one more valence electron than that of Fe, the VEC of $MFe_{1-x}Co_xSb$ samples changes according to the Fe/Co ratio. As shown in Fig. 2(b), a pure HH phase is achieved for the compounds with VEC from 17.9 to 18.5, which provides an effective means to tune the properties of the high-entropy HH.

Fig. 3(a) shows a typical fracture surface of a representative sample of $MFe_{0.5}Co_{0.5}Sb$. The sample is dense with fine grain size of 50–500 nm. The grain size is much smaller than that reported for samples prepared using traditional methods, for which the typical grain size is in microns. The fine grain size in this work benefits from the synthesis method of ball-milling and rapid SPS. Fig. 3(b) shows a backscattered electron image of a polished surface and Fig. 3(c) shows the corresponding EDX mapping results. The composition based on the EDX results is $Ti_{0.17}Zr_{0.16}Hf_{0.16}V_{0.15}Nb_{0.17}Ta_{0.18}Fe_{0.46}Co_{0.45}Sb$, which is very close to the nominal composition. High magnification SEM and EDX results are shown in Fig. S2 (Support Information), and the EDX results show similar composition. There is no obvious impurity or phase separation in the sample and all of the elements are homogeneously distributed. However, a trace amount of unreacted Hf was observed when the sample was scanned carefully (See Fig. S3 in Support information). A summary of EDX results of all the compositions are shown in Table S1 (Support Information). The XRD, SEM and EDX results indicate that a high-entropy HH was formed.

The temperature dependent electrical transport properties of $MFe_{1-x}Co_xSb$ (x = 0.3, 0.4, 0.5, 0.6 and 1.0) are shown in Fig. 4. The $MFe_{0.5}Co_{0.5}Sb$ sample (x = 0.5) with 18 VEC shows intrinsic semiconducting behavior with a relatively low electrical conductivity that increases with increasing temperature. It has a negative Seebeck coefficient indicating that it is an n-type semi-conductor, but the absolute value of Seebeck coefficient (~ −70 μVK^{-1}) is relatively low compared with intrinsic n-type HH TiNiSn (~ −250 μVK^{-1}) [5]. The electrical properties were tuned by changing the Fe/Co ratio. Since Co has one more valence electron than that of Fe, more Co should introduce electrons while more Fe should introduce holes. For the $MFe_{0.4}Co_{0.6}Sb$ (x = 0.6) and MCoSb (x = 1.0) samples with more Co than Fe (n-type doped), the electrical conductivities and the Seebeck coefficients were increased simultaneously compared with those of the $MFe_{0.5}Co_{0.5}Sb$ sample. The MCoSb sample (VEC 18.5) shows a Seebeck coefficient of ~ −200 μVK^{-1} at 923 K, which is largely

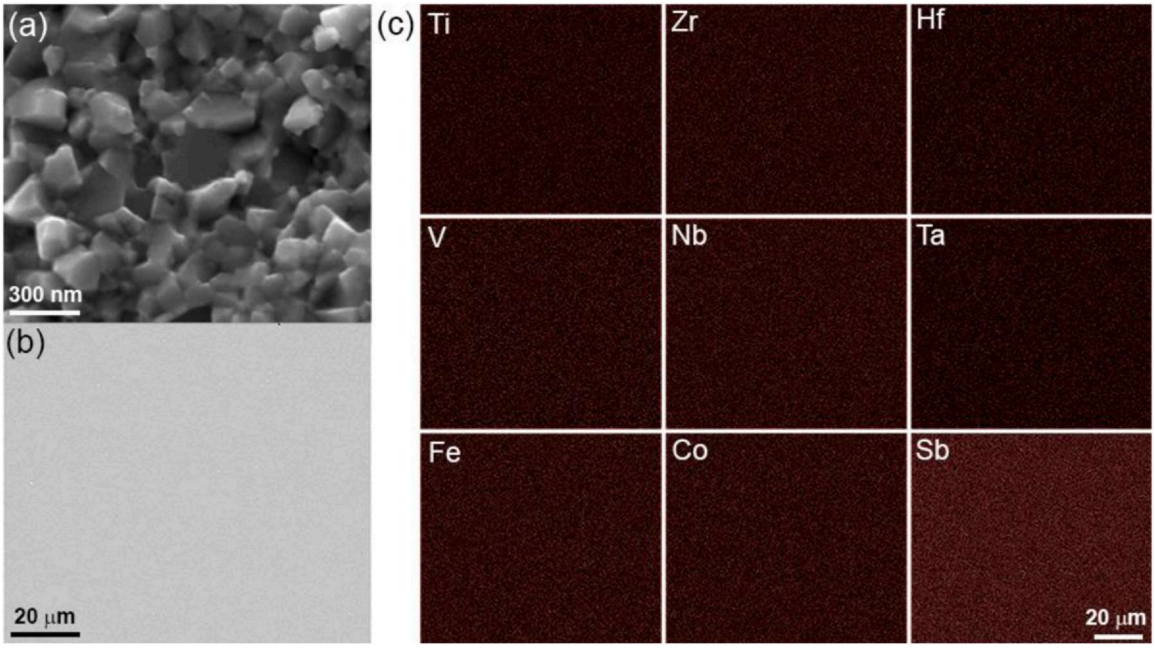

Fig. 3. (a) SEM image of fractured surface, (b) Backscattered electron image of polished surface and (c) EDX mapping of polished surface, for a representative sample $MFe_{0.5}Co_{0.5}Sb$ (M = equimolar Ti, Zr, Hf, V, Nb, Ta). The composition based on the EDX results is $Ti_{0.17}Zr_{0.16}Hf_{0.16}V_{0.15}Nb_{0.17}Ta_{0.18}Fe_{0.46}Co_{0.45}Sb$, which is very close to the nominal composition.

enhanced and comparable to the values reported for good n-type HH compounds. This improvement might correlate to their band structures, as changes or substitutions of the Y elements can be expected to engineer the bandgap and effective mass based on the Zintl concept [9]. For the $MFe_{0.6}Co_{0.4}Sb$ ($x = 0.4$) and $MFe_{0.7}Co_{0.3}Sb$ ($x = 0.3$) samples with more Fe than Co (p-type doped), the electrical conductivities were significantly increased compared with that of the $MFe_{0.5}Co_{0.5}Sb$ sample and the samples were tuned into p-type conductors with positive Seebeck coefficients. A maximum value of ~ +175 μVK^{-1} was achieved in $MFe_{0.6}Co_{0.4}Sb$, which is comparable with

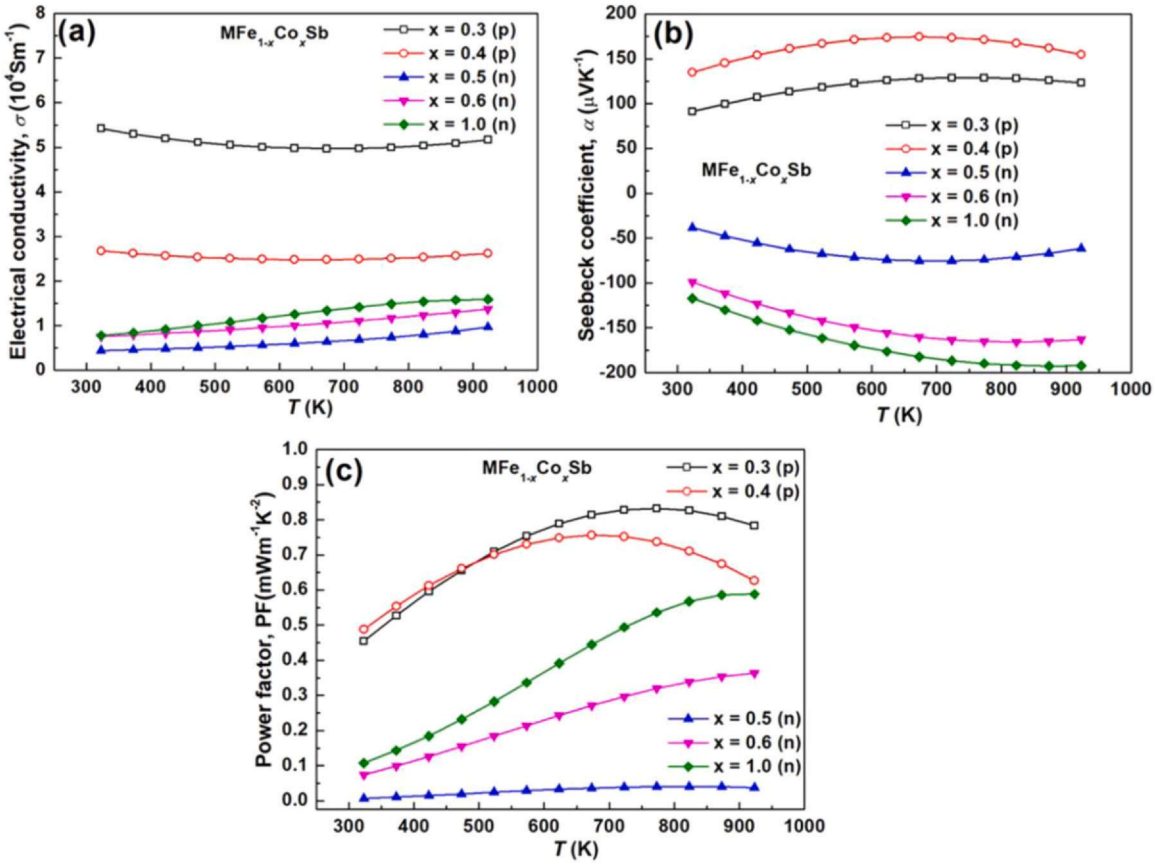

Fig. 4. Temperature dependent electrical transport properties of $MFe_{1-x}Co_xSb$ (M = equimolar Ti, Zr, Hf, V, Nb, Ta), (a) electrical conductivity, (b) Seebeck coefficient and (c) power factor.

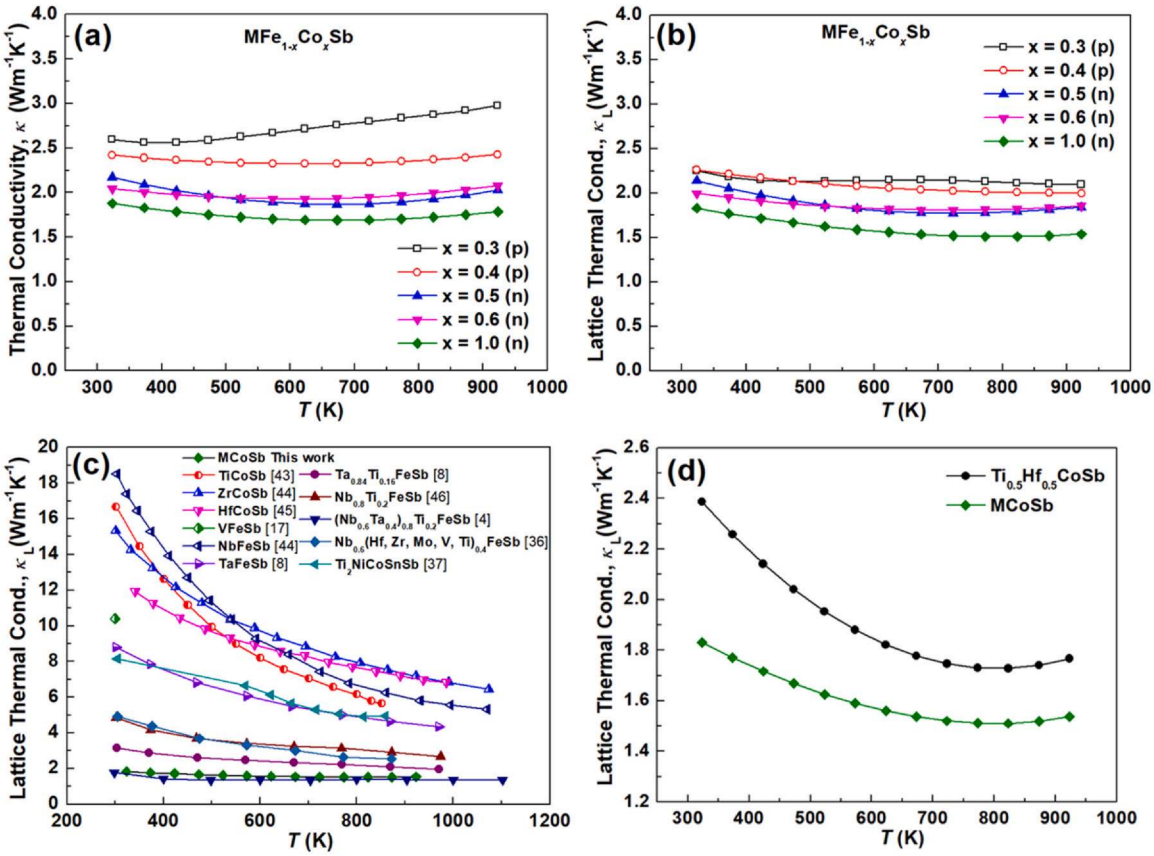

Fig. 5. Temperature dependent thermal transport properties of $MFe_{1-x}Co_xSb$ (M = equimolar Ti, Zr, Hf, V, Nb, Ta), (a) thermal conductivity, (b) lattice thermal conductivity, (c) comparison of lattice thermal conductivity of MCoSb with reported results for Sb-based half-Heusler, and (d) comparison of lattice thermal conductivity of MCoSb with $Ti_{0.5}Hf_{0.5}CoSb$ prepared by same method.

reported values for p-type HH (NbFeSb) [4,41]. It is worth noting that the high-entropy HH $MFe_{1-x}Co_xSb$ can exhibit both n-type and p-type behaviors by simply adjusting the Fe/Co ratio and show decent Seebeck coefficients. Although the electrical conductivities of both the n-type and p-type samples are relatively low leading to lower power factors compared with those of traditional HH compounds, the use of optimized dopants could further improve the power factors.

The temperature dependent thermal conductivities (κ) and lattice thermal conductivities (κ_L) of $MFe_{1-x}Co_xSb$ ($x = 0.3$, 0.4, 0.5, 0.6 and 1.0) are shown in Fig. 5(a) and (b). The measured thermal diffusivity results are shown in Fig. S4 (Support Information). Both p-type samples (x = 0.3 and 0.4) have higher thermal conductivities due to their higher electrical conductivities. The $x = 0.3$ sample has a different temperature dependence compared with all other samples, which is probably caused by the impurities in this sample. The thermal conductivities of all other samples first decrease and then increase with increasing temperature indicating bipolar effects. The lattice thermal conductivity (κ_L) was calculated by subtracting the electronic thermal conductivity (κ_e) from κ with κ_e calculated using the Wiedemann–Franz law, $\kappa_e = LT\sigma$, where L is the Lorenz number. L was estimated by using the empirical expression L = 1.5+ exp [116 /|α|] [42]. The lattice thermal conductivity of samples with different Fe/Co ratio are similar; as Fe and Co have very similar atomic mass and size, which is not expected to have obvious effect on lattice thermal conductivity. The lowest κ_L is about 1.8–1.5 $Wm^{-1}K^{-1}$ from 300 K to 923 K. As shown in Fig. 5(c), the κ_L of MCoSb is much lower than the reported values of Sb-based half-Heusler compounds with single element on the X site (TiCoSb [43], ZrCoSb [44], HfCoSb [45], VFeSb [17], NbFeSb [44] and TaFeSb [8]). It is also lower than the reported values for the two compounds containing multi-elements ($Nb_{0.6}$(Hf, Zr, Mo, V, Ti)$_{0.4}$FeSb [36] and Ti_2NiCoSnSb [37]), and some of the reported Sb-based half-Heusler compounds with very low κ_L ($Ta_{0.84}Ti_{0.16}$FeSb [8], ($Nb_{0.6}Ta_{0.4}$)$_{0.8}Ti_{0.2}$FeSb [4], $Nb_{0.8}Ti_{0.2}$FeSb [46]). The results indicate that high-entropy effects are very effective in reducing lattice thermal conductivity. This is further highlight when comparing the lattice thermal conductivity of MCoSb with $Ti_{0.5}Hf_{0.5}CoSb$ prepared by the same processing route (Fig. 5(d)). While the choice of Ti and Hf on the X site maximizes the mass contrast effect [47,48], the high-entropy HH MCoSb still has significantly lower lattice thermal conductivity.

Fig. 6 shows the temperature dependence of the figure of merit, *zT*. Maximum *zT* values of 0.25 and 0.3 are achieved for p-type $MFe_{0.6}Co_{0.4}Sb$ and n-type MCoSb, respectively. Although the zT

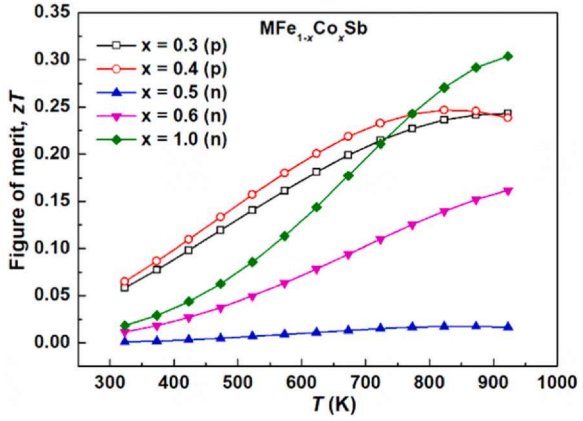

Fig. 6. Temperature dependent zT of $MFe_{1-x}Co_xSb$ (M = equimolar Ti, Zr, Hf, V, Nb, Ta).

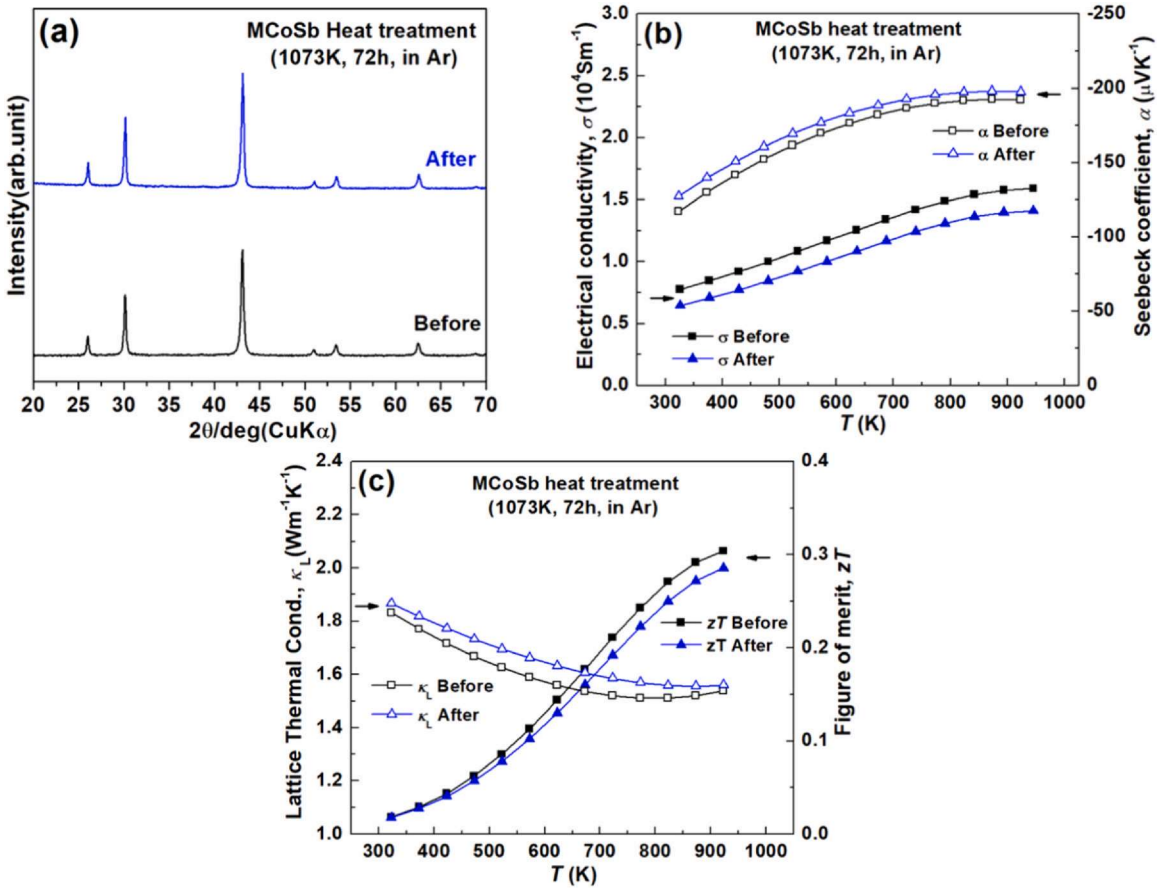

Fig. 7. Comparisons of XRD and thermoelectric properties of MCoSb (M = equimolar Ti, Zr, Hf, V, Nb, Ta) before and after heat treatment at 1073 K for 72 h in Ar.

values are low compared with the state-of-the-art HH TE materials, there is space for further improvement of the electrical properties with the use of effective dopants. The thermal stability of MCoSb was tested by heat treating the sample at 1073 K for 72 h under flowing Ar. The XRD and thermoelectric properties of MCoSb before and after heat treatment are shown in Fig. 7. There is no phase separation or impurities after heat treatment and the thermoelectric properties are consistent, which indicates the high-entropy HH is thermally stable up to 1073 K in Ar.

4. Conclusions

High-entropy HH compounds of $MFe_{1-x}Co_xSb$ (M= equimolar Ti, Zr, HF, V, Nb, Ta) were successfully prepared by a fast and scalable method of ball-milling and rapid SPS consolidation. XRD and EDX results indicates high purity and homogeneity, despite the fact that the atomic radius of the smallest atom (V) and the largest atom (Zr) differ by more than 15%. The six equimolar elements in the X cation sublattice, which have large configurational entropy, could contribute to the formation of a single-phase. $MFe_{1-x}Co_xSb$ system showed great tunability. A pure HH phase was maintained with VEC from 17.9 to 18.5, and the system can behave as both n- and p-type according to the VEC. A very low lattice thermal conductivity of 1.8–1.5 $Wm^{-1}K^{-1}$ (300–923 K) was achieved for MCoSb, probably due to mass contrast and point defects introduced by multiple elements. Maximum zT values of 0.25 and 0.3 are achieved for p-type $MFe_{0.6}Co_{0.4}Sb$ and n-type MCoSb, respectively. The high-entropy HH samples are reproducible and heat treatment indicates that the samples have good thermal stability (up to 1073 K), which is attributed to their high configurational entropy. The high-entropy concept is a promising strategy to extend the composition range, suppress the lattice thermal conductivity and tune the electrical properties of half-Heusler materials, which could potentially be applied in other thermoelectric materials.

CRediT authorship contribution statement

Kan Chen: Conceptualization, Methodology, Investigation, Writing – original draft. **Ruizhi Zhang**: Formal analysis, Writing – review & editing. **Jan-Willem G. Bos**: Writing – review & editing. **Michael J. Reece**: Conceptualization, Resources, Writing – review & editing, Supervision, Funding acquisition.

Declaration of Competing Interest

The authors declare that they have no known competing financial interests or personal relationships that could have appeared to influence the work reported in this paper.

Acknowledgement

We gratefully acknowledge the support from European Thermodynamics Ltd. J-W. G. B acknowledges Engineering and Physical Sciences Research Council (EPSRC) (Grant No. EP/N01717X/1).

Appendix A. Supporting information

Supplementary data associated with this article can be found in the online version at doi:10.1016/j.jallcom.2021.162045.

References

[1] D.M. Rowe, Crc Handbook of Thermoelectrics, CRC Press,, 1995.
[2] G.S. Nolas, J. Sharp, H.J. Goldsmid, Thermoelectrics, Springer,, Berlin, Heidelberg, 2001.
[3] Z. Tian, S. Lee, G. Chen, Comprehensive review of heat transfer in thermoelectric materials and devices, Annu. Rev. Heat. Transf. 17 (2014) 425–483.
[4] J. Yu, C. Fu, Y. Liu, K. Xia, U. Aydemir, T.C. Chasapis, G.J. Snyder, X. Zhao, T. Zhu, Unique role of refractory Ta alloying in enhancing the figure of merit of NbFeSb thermoelectric materials, Adv. Energy Mater. 8 (2017) 1701313.
[5] K. Chen, C. Nuttall, E. Stefanaki, K. Placha, R. Tuley, K. Simpson, J.-W.G. Bos, M.J. Reece, Fast synthesis of n-type half-heusler tinisn thermoelectric material, Scr. Mater. 191 (2021) 71–75.
[6] S.J. Poon, Half heusler compounds: promising materials for mid-to-high temperature thermoelectric conversion, J. Phys. D: Appl. Phys. 52 (2019) 493001.
[7] D. Landmann, Y.L. Tang, B. Kunz, R. Huber, D. Widner, P. Rickhaus, R.N. Widmer, H.R. Elsener, C. Battaglia, Fabrication, characterization, and application-matched design of thermoelectric modules based on half-heusler fenbsb and tinisn, J. Appl. Phys. 126 (2019) 085113.
[8] H. Zhu, J. Mao, Y. Li, J. Sun, Y. Wang, Q. Zhu, G. Li, Q. Song, J. Zhou, Y. Fu, R. He, T. Tong, Z. Liu, W. Ren, L. You, Z. Wang, J. Luo, A. Sotnikov, J. Bao, K. Nielsch, G. Chen, D.J. Singh, Z. Ren, Discovery of tafesb-based half-heuslers with high thermoelectric performance, Nat. Commun. 10 (2019) 270.
[9] W.G. Zeier, J. Schmitt, G. Hautier, U. Aydemir, Z.M. Gibbs, C. Felser, G.J. Snyder, Engineering half-heusler thermoelectric materials using Zintl chemistry, Nat. Rev. Mater. 1 (2016) 16032.
[10] X. Yan, W. Liu, H. Wang, S. Chen, J. Shiomi, K. Esfarjani, H. Wang, D. Wang, G. Chen, Z. Ren, Stronger phonon scattering by larger differences in atomic mass and size in P-type Half-Heuslers $Hf_{1-x}ti_xcosb_{0.8}sn_{0.2}$, Energy Environ. Sci. 5 (2012) 7543–7548.
[11] M. Gürth, G. Rogl, V.V. Romaka, A. Grytsiv, E. Bauer, P. Rogl, Thermoelectric high Zt Half-Heusler alloys $Ti_{1-x-y}Zr_xh_fynisn$ ($0 \le x \le 1$; $0 \le y \le 1$), Acta Mater. 104 (2016) 210–222.
[12] T. Zhu, C. Fu, H. Xie, Y. Liu, X. Zhao, High efficiency Half-Heusler thermoelectric materials for energy harvesting, Adv. Energy Mater. 5 (2015) 1500588.
[13] G. Rogl, K. Yubuta, V.V. Romaka, H. Michor, E. Schafler, A. Grytsiv, E. Bauer, P. Rogl, High-Zt Half-Heusler thermoelectrics, $Ti_{0.5}zr_{0.5}nisn$ and $Ti_{0.5}zr_{0.5}nisn_{0.98}sb_{0.02}$: physical properties at low temperatures, Acta Mater. 166 (2019) 466–483.
[14] C. Fu, T. Zhu, Y. Pei, H. Xie, H. Wang, G.J. Snyder, Y. Liu, Y. Liu, X. Zhao, High band degeneracy contributes to high thermoelectric performance in P-type Half-Heusler compounds, Adv. Energy Mater. 4 (2014) 1400600.
[15] C. Fu, S. Bai, Y. Liu, Y. Tang, L. Chen, X. Zhao, T. Zhu, Realizing high figure of merit in heavy-band P-type Half-Heusler thermoelectric materials, Nat. Commun. 6 (2015) 8144.
[16] R. He, L. Huang, Y. Wang, G. Samsonidze, B. Kozinsky, Q. Zhang, Z. Ren, Enhanced thermoelectric properties of N-Type Nbcosn Half-Heusler by improving phase purity, APL Mater. 4 (2016) 104804.
[17] Y. Stadnyk; L. Romaka; Y. Gorelenko; A. Tkachuk; J. Pierre In Crystal Structure and Electrokinetic Properties of Vfesb Compound, Proceedings ICT2001. 20 International Conference on Thermoelectrics (Cat. No.01TH8589), 8–11 June 2001; 2001; pp 251–253.
[18] H. Zhu, R. He, J. Mao, Q. Zhu, C. Li, J. Sun, W. Ren, Y. Wang, Z. Liu, Z. Tang, A. Sotnikov, Z. Wang, D. Broido, D.J. Singh, G. Chen, K. Nielsch, Z. Ren, Discovery of Zrcobi based Half Heuslers with high thermoelectric conversion efficiency, Nat. Commun. 9 (2018) 2497.
[19] D. Zhao, M. Zuo, L. Bo, Y. Wang, Synthesis and thermoelectric properties of Pd-doped ZrCoBi Half-Heusler compounds, Materials 11 (2018) 728.
[20] R. Gautier, X. Zhang, L. Hu, L. Yu, Y. Lin, T.O.L. Sunde, D. Chon, K.R. Poeppelmeier, A. Zunger, Prediction and accelerated laboratory discovery of previously unknown 18-electron Abx compounds, Nat. Chem. 7 (2015) 308–316.
[21] J.-W. Yeh, S.-K. Chen, S.-J. Lin, J.-Y. Gan, T.-S. Chin, T.-T. Shun, C.-H. Tsau, S.-Y. Chang, Nanostructured high-entropy alloys with multiple principal elements: novel alloy design concepts and outcomes, Adv. Eng. Mater. 6 (2004) 299–303.
[22] B. Cantor, I.T.H. Chang, P. Knight, A.J.B. Vincent, Microstructural development in equiatomic multicomponent alloys, Mater. Sci. Eng.: A 375–377 (2004) 213–218.
[23] Z. Lei, X. Liu, Y. Wu, H. Wang, S. Jiang, S. Wang, X. Hui, Y. Wu, B. Gault, P. Kontis, D. Raabe, L. Gu, Q. Zhang, H. Chen, H. Wang, J. Liu, K. An, Q. Zeng, T.-G. Nieh, Z. Lu, Enhanced strength and ductility in a high-entropy alloy via ordered oxygen complexes, Nature 563 (2018) 546–550.
[24] S. Jiang, T. Hu, J. Gild, N. Zhou, J. Nie, M. Qin, T. Harrington, K. Vecchio, J. Luo, A. New, Class of high-entropy perovskite oxides, Scr. Mater. 142 (2018) 116–120.
[25] C.M. Rost, E. Sachet, T. Borman, A. Moballegh, E.C. Dickey, D. Hou, J.L. Jones, S. Curtarolo, J.-P. Maria, Entropy-stabilized oxides, Nat. Commun. 6 (2015) 8485.
[26] T.-K. Chen, M.-S. Wong, T.-T. Shun, J.-W. Yeh, Nanostructured nitride films of multi-element high-entropy alloys by reactive Dc sputtering, Surf. Coat. Technol. 200 (2005) 1361–1365.
[27] E. Castle, T. Csanádi, S. Grasso, J. Dusza, M. Reece, Processing and properties of high-entropy ultra-high temperature carbides, Sci. Rep. 8 (2018) 8609.
[28] M. Biesuz, T.G. Saunders, K. Chen, M. Bortolotti, M. Salvo, S. Grasso, M.J. Reece, Interfacial reaction between ZrNbHfTa Foil And Graphite: Formation Of High-entropy Carbide And The Effect Of Heating Rate On Its Microstructure, J. Eur. Ceram. Soc. 40 (2020) 2699–2708.
[29] J. Gild, Y. Zhang, T. Harrington, S. Jiang, T. Hu, M.C. Quinn, W.M. Mellor, N. Zhou, K. Vecchio, J. Luo, High-entropy metal diborides: a new class of high-entropy materials and a new type of ultrahigh temperature ceramics, Sci. Rep. 6 (2016) 37946.
[30] R. Liu, H. Chen, K. Zhao, Y. Qin, B. Jiang, T. Zhang, G. Sha, X. Shi, C. Uher, W. Zhang, L. Chen, Entropy as a gene-like performance indicator promoting thermoelectric materials, Adv. Mater. 29 (2017) 17027121702712-n/a.
[31] R.-Z. Zhang, F. Gucci, H. Zhu, K. Chen, M.J. Reece, Data-driven design of ecofriendly thermoelectric high-entropy sulfides, Inorg. Chem. 57 (2018) 13027–13033.
[32] R.-Z. Zhang, M.J. Reece, Review of high entropy ceramics: design, synthesis, structure and properties, J. Mater. Chem. A 7 (2019) 22148–22162.
[33] D. Bérardan; S. Franger; D. Dragoe; A.K. Meena; N. Dragoe, Colossal Dielectric Constant in High Entropy Oxides. physica status solidi (RRL) – Rapid Research Letters 2016, 10, 328–333.
[34] D. Bérardan, S. Franger, A.K. Meena, N. Dragoe, Room temperature lithium superionic conductivity in high entropy oxides, J. Mater. Chem. A 4 (2016) 9536–9541.
[35] A. Sarkar, L. Velasco, D. Wang, Q. Wang, G. Talasila, L. de Biasi, C. Kübel, T. Brezesinski, S.S. Bhattacharya, H. Hahn, B. Breitung, High entropy oxides for reversible energy storage, Nat. Commun. 9 (2018) 3400.
[36] J. Yan, F. Liu, G. Ma, B. Gong, J. Zhu, X. Wang, W. Ao, C. Zhang, Y. Li, J. Li, Suppression of the lattice thermal conductivity in nbfesb-based Half-Heusler thermoelectric materials through high entropy effects, Scr. Mater. 157 (2018) 129–134.
[37] A. Karati, M. Nagini, S. Ghosh, R. Shabadi, K.G. Pradeep, R.C. Mallik, B.S. Murty, U.V. Varadaraju, Ti2nicosnsb - a new Half-Heusler type high-entropy alloy showing simultaneous increase in seebeck coefficient and electrical conductivity for thermoelectric applications, Sci. Rep. 9 (2019) 5331.
[38] J. Liu, G. Shao, D. Liu, K. Chen, K. Wang, B. Ma, K. Ren, Y. Wang, Design and synthesis of chemically complex ceramics from the perspective of entropy, Mater. Today Adv. 8 (2020) 100114.
[39] W.D. Callister, D.G. Rethwisch, Materials Science and Engineering: An Introduction Vol. 9 Wiley,, New York, 2018.
[40] E. Rausch, B. Balke, T. Deschauer, S. Ouardi, C. Felser, Charge carrier concentration optimization of thermoelectric P-type Half-Heusler compounds, APL Mater. 3 (2015) 041516.
[41] G. Joshi, R. He, M. Engber, G. Samsonidze, T. Pantha, E. Dahal, K. Dahal, J. Yang, Y. Lan, B. Kozinsky, Z. Ren, Nbfesb-based P-type Half-Heuslers for power generation applications, Energy Environ. Sci. 7 (2014) 4070–4076.
[42] H.S. Kim, Z.M. Gibbs, Y.L. Tang, H. Wang, G.J. Snyder, Characterization of Lorenz number with seebeck coefficient measurement, APL Mater. 3 (2015) 041506.
[43] T. Wu, W. Jiang, X. Li, S. Bai, S. Liufu, L. Chen, Effects of Ge doping on the thermoelectric properties of TiCoSb-based P-type Half-Heusler compounds, J. Alloy. Compd. 467 (2009) 590–594.
[44] W. Silpawilawan, K. Kurosaki, Y. Ohishi, H. Muta, S. Yamanaka, Fenbsb P-type Half-Heusler compound: beneficial thermomechanical properties and high-temperature stability for thermoelectrics, J. Mater. Chem. C. 5 (2017) 6677–6681.
[45] T. Sekimoto; K. Kurosaki; H. Muta; S. Yamasaka In thermoelectric and thermophysical properties of TiCoSb, ZrCoSb, HfCoSb prepared by Sps, ICT 2005, in: Proceedings of the 24th International Conference on Thermoelectrics, 2005., 19–23 June 2005; 2005; pp 347–350.
[46] R. He; D. Kraemer; J. Mao; L. Zeng; Q. Jie; Y. Lan; C. Li; J. Shuai; H.S. Kim; Y. Liu; D. Broido; C.-W. Chu; G. Chen; Z. Ren, Achieving High Power Factor and Output Power Density in P-Type Half-Heuslers $Nb_{1-x}ti_xfesb$. Proceedings of the National Academy of Sciences 2016, 113, 13576–13581.
[47] E.S. Toberer, A. Zevalkink, G.J. Snyder, Phonon engineering through crystal chemistry, J. Mater. Chem. 21 (2011) 15843.
[48] R. Gurunathan, R. Hanus, G.J. Snyder, Alloy scattering of phonons, Mater. Horiz. 7 (2020) 1452–1456.